NANO LETTERS

Letter

pubs.acs.org/NanoLett

Defect Healing and Charge Transfer-Mediated Valley Polarization in $MoS_2/MoSe_2/MoS_2$ Trilayer van der Waals Heterostructures

Alessandro Surrente,[†] Dumitru Dumcenco,[‡] Zhuo Yang,[†] Agnieszka Kuc,[§,∥] Yu Jing,[§] Thomas Heine,[§,∥] Yen-Cheng Kung,[‡] Duncan K. Maude,[†] Andras Kis,[‡] and Paulina Plochocka*[,†]

[†]Laboratoire National des Champs Magnétiques Intenses, UPR 3228, CNRS-UGA-UPS-INSA, Grenoble and Toulouse, France

[‡]Electrical Engineering Institute and Institute of Materials Science and Engineering, École Polytechnique Fédérale de Lausanne, CH-1015 Lausanne, Switzerland

[§]Wilhelm Ostwald Institute of Physical and Theoretical Chemistry Leipzig, University of Leipzig, 04109 Saxony Germany

[∥]School of Engineering and Science, Jacobs University Bremen, Campus Ring 1, 28759 Bremen, Germany

Supporting Information

ABSTRACT: Monolayer transition metal dichalcogenides (TMDCs) grown by chemical vapor deposition (CVD) are plagued by a significantly lower optical quality compared to exfoliated TMDCs. In this work, we show that the optical quality of CVD-grown $MoSe_2$ is completely recovered if the material is sandwiched in $MoS_2/MoSe_2/MoS_2$ trilayer van der Waals heterostructures. We show by means of density functional theory that this remarkable and unexpected result is due to defect healing: S atoms of the more reactive MoS_2 layers are donated to heal Se vacancy defects in the middle $MoSe_2$ layer. In addition, the trilayer structure exhibits a considerable charge-transfer mediated valley polarization of $MoSe_2$ without the need for resonant excitation. Our fabrication approach, relying solely on simple flake transfer technique, paves the way for the scalable production of large-area TMDC materials with excellent optical quality.

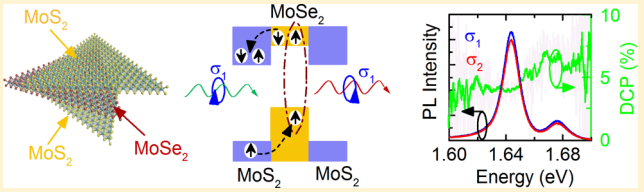

KEYWORDS: *Chemical vapor deposition, transition metal dichalcogenides, van der Waals heterostructures, defect healing, charge transfer mediated valley polarization*

Monolayer transition metal dichalcogenides (TMDC) have a direct bandgap situated in the visible range, which makes them ideal building blocks for novel electronic and optoelectronic devices.[1−10] The bandgap of monolayer TMDCs occurs at the inequivalent (but degenerate) K and K′ points of the hexagonal Brillouin zone. The broken inversion symmetry of a TMDC monolayer combined with the time reversal symmetry imposes opposite magnetic moments at the K and K′ valleys. This in turn determines the characteristic circular dichroism exhibited by these materials, wherein each valley can be addressed separately with circularly polarized light of a given helicity.[11−13] Additionally, optical spectra are influenced by the strong spin−orbit coupling, which lifts the degeneracy of band states at the valence band edges, resulting in well-resolved A and B resonances, as observed in reflectivity or absorption spectra.[2,14−16] The interplay of spin−orbit coupling with broken inversion symmetry and time reversal symmetry locks the valley and spin degrees of freedom, making TMDCs attractive candidates for valleytronics.[17] The spin-valley index locking along with the large distance in the momentum space between K and K′ valleys preserves the valley polarization observed in the degree of circular polarization (DCP) in helicity resolved photoluminescence emission.[18−22]

Applications require a scalable fabrication platform providing high-quality large-area monolayer TMDC. Unfortunately, the most promising approach today, namely chemical vapor deposition (CVD) growth[23−27] struggles to compete with exfoliated TMDCs in terms of sample quality. Low-temperature photoluminescence (PL) spectroscopy of CVD-grown MoS_2 and $MoSe_2$ reveals broad emission from defect bound excitons, which is significantly more intense than the free exciton peak[28−30] and is related to chalcogen vacancies induced during the CVD growth.[29,30]

Here, we demonstrate a novel approach to neutralize the intrinsic defects of CVD-grown TMDCs, using flake transfer tools routinely employed in the fabrication of van der Waals heterostructures.[31−33] We investigate the optical properties of trilayer stacks composed of external CVD-grown MoS_2 flakes[24] as capping layers and an internal CVD-grown $MoSe_2$ flake that has a smaller bandgap.[34,35] Remarkably, this fabrication approach strongly suppresses the localized exciton emission in $MoSe_2$, yielding a low-temperature PL comparable to that observed in mechanically exfoliated samples. This striking result can be understood from density functional theory (DFT), which suggests that the more reactive MoS_2 donates chalcogen atoms to heal vacancy defects in $MoSe_2$. Incorporating MoS_2

Received: March 2, 2017
Revised: June 9, 2017
Published: June 12, 2017

DOI: 10.1021/acs.nanolett.7b00904
Nano Lett. XXXX, XXX, XXX−XXX

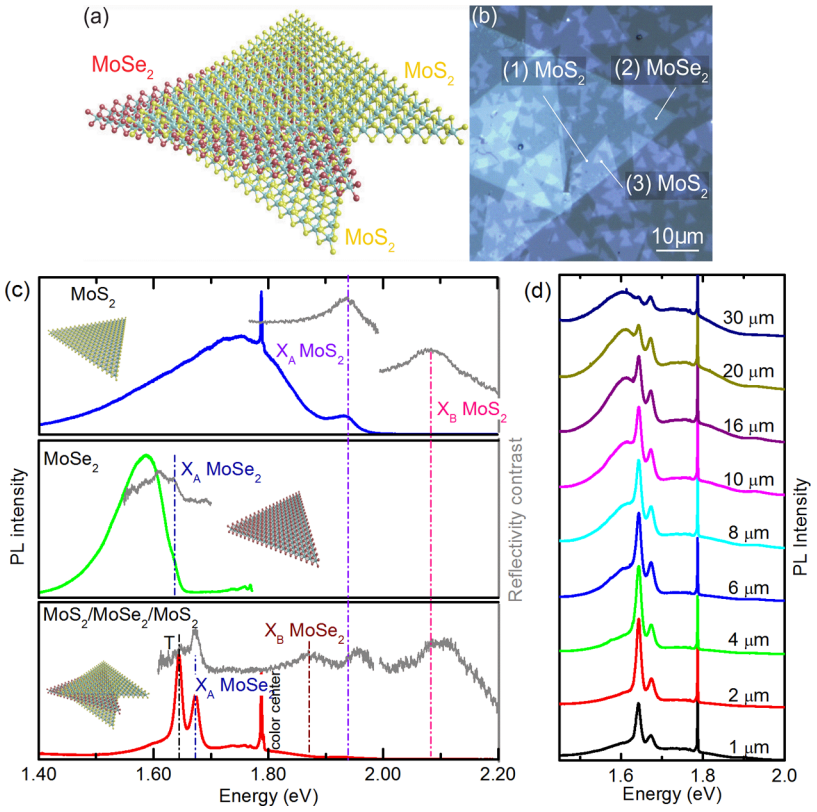

Figure 1. (a) Ball and stick model of $MoSe_2$ layer sandwiched between two MoS_2 flakes. (b) Optical micrograph of a representative transfer area. (c) Low-temperature μPL spectra (colored curves) and reflectivity contrast (gray curves) of as-grown MoS_2, $MoSe_2$ monolayers and $MoS_2/MoSe_2/MoS_2$ trilayer stack. (d) PL spectra of trilayer stack measured using different spot sizes. The spectra are vertically offset for clarity. X_A indicates A exciton and T denotes the trion (charged A exciton).

into the trilayer heterostructure furthermore allows us to demonstrate a new way to introduce valley polarization in $MoSe_2$. Because of the type II band alignment in TMDC heterojunctions,[35] a significant charge transfer is observed in these systems.[32,36,37] Our results show that spin of the hole is conserved upon charge transfer from MoS_2 to $MoSe_2$ after excitation in resonance with MoS_2 A exciton. This leads to nonzero steady-state valley polarization in $MoSe_2$, which has never been observed before under nonresonant excitation.[38−40]

Defect Healing. The sample with $MoS_2/MoSe_2/MoS_2$ trilayer stacks and micrograph of a representative transfer area are schematically shown in Figure 1a,b. Low-temperature microPL (μPL) spectroscopy has been used to characterize as-grown CVD samples on the sapphire substrate (prior to any transfer process) and the trilayer $MoS_2/MoSe_2/MoS_2$ stack. All spectra shown in Figure 1c,d were measured under nominally identical conditions with an excitation power of 100 μW (see Figure S1 in Supporting Information (SI) for power dependent μPL spectra). The as-grown MoS_2 and $MoSe_2$ monolayers both show a broad PL feature (full width at half-maximum, fwhm, of 258 and 106 meV, respectively) related to emission from excitons bound to defect or charge impurity states.[28−30,41] A-exciton emission (labeled X_A in Figure 1c) is seen only as a weak peak or shoulder at higher energies. These assignments are confirmed by reflectivity contrast measured on the same spot. Reflectivity contrast is defined as $\Delta R/R_s = (R - R_s)/R_s$, where R is the reflectivity spectrum measured on the sample and R_s denotes the reflectivity spectrum measured on the substrate. In the case of transparent substrates such as sapphire, reflectivity contrast is proportional to the absorption of the sample.[42] The reflectivity contrast spectrum of as-grown MoS_2 (see upper panel of Figure 1c) consists of a main peak at 1.937 eV and a higher energy, weaker feature at 2.085 eV, related to the spin−orbit split B exciton. The energy difference of 148 meV corresponds very well to theoretically predicted spin−orbit splitting of the valence band[43] and is very similar to the splitting determined with transmission measurements on similar samples.[34] The reflectivity contrast spectrum of as-grown $MoSe_2$, shown in the central panel of Figure 1c has a peak at 1.637 eV, which corresponds well to the high energy shoulder of the μPL spectrum and hence is assigned to A exciton. As in our previous study,[34] we are unable to resolve the B exciton in reflectivity contrast measurements on as grown $MoSe_2$.

The optical properties of the trilayer stack are dramatically improved (bottom panel in Figure 1c). The most striking difference is the nearly total suppression of (i) emission from defect bound excitons, and (ii) significant quenching of both MoS_2 PL, barely seen as a weak peak at 1.929 eV, and of $MoSe_2$ PL (overall integrated intensity decreases by two and one orders of magnitude, respectively, see Figure S2 in SI). The measured PL spectrum is dominated by narrow free neutral (X_A) and charged exciton (T) emission in $MoSe_2$ (low power fwhm of 11 and 10 meV, respectively, see Figure S1 in SI), approaching the quality of exfoliated WSe_2 embedded in boron nitride (fwhm ~10 meV).[44] The free exciton emission overlaps with a weak broad background emission from the sapphire substrate (the narrow peak just below 1.8 eV corresponds to the emission from a color center in sapphire). The highest energy peak in the reflectivity contrast spectrum of the trilayer

DOI: 10.1021/acs.nanolett.7b00904
Nano Lett. XXXX, XXX, XXX−XXX

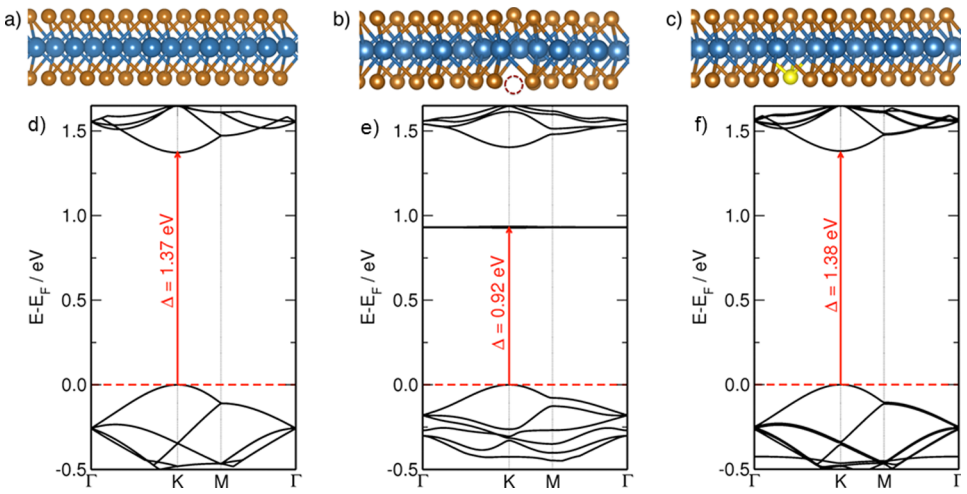

Figure 2. (a–c) Atomic representation of a perfect $MoSe_2$ monolayer, the $MoSe_2$ monolayer with 1 Se vacancy, and the $MoSe_2$ monolayer with 1 S substitution, respectively. (d–f) Corresponding calculated band structures. Fermi level (horizontal dashed lines) is shifted to the top of the valence band. Fundamental bandgaps are indicated.

(see Figure 1c, bottom panel), blue-shifted with respect to the A exciton peak of MoS_2 by 145 meV is attributed to the B exciton of MoS_2. The peak related to MoS_2 A exciton in the reflectivity contrast spectrum is blue-shifted by 27 meV with respect to the corresponding PL peak. This Stokes shift has been attributed to the presence of a high doping level in MoS_2,[16] also present in our layers.[45] On the low energy side of the μPL spectrum, the two distinct peaks at 1.674 and 1.645 eV are assigned to the A exciton and to the trion of $MoSe_2$, respectively. The trion binding energy of 29 meV is very similar to that reported in other studies on $MoSe_2$.[29,46]

The high optical quality of the $MoSe_2$ embedded in the heterostructure enabled us to resolve an additional peak at 1.87 eV in the reflectivity contrast spectrum, assigned to the B exciton of $MoSe_2$.[43,47] The vastly improved optical properties suggest a defect healing process in which the contact with MoS_2 is enough to drastically reduce the number of defects in $MoSe_2$. The quenching of the intralayer emission[32,37] in the trilayer is manifestation of a fast charge transfer mechanism[36,48] related to the type II band alignment in $MoS_2/MoSe_2$ heterostructures.[35] The weak luminescence of MoS_2 is consistent with a background n-doping[45] of the as grown layers and with an additional charge transfer after the formation of the heterostructure. We assign the brighter emission from $MoSe_2$ (in the trilayer) to the hole transfer to an intrinsically n-doped material and to the defect healing effect, combined with luminescence resulting from higher energy states, similar to hot luminescence of direct exciton in multilayer $MoSe_2$.[49,50] The long-range optical uniformity of the trilayer stacks has been monitored by acquiring PL with a gradually defocused excitation beam. The acquired PL spectra are displayed in Figure 1d. For an excitation spot size of 10 μm, the defect emission remains strongly suppressed. For larger spot sizes, a broad low-energy peak starts to emerge, probably due to defect related emission in $MoSe_2$ in areas which are not fully capped. These measurements are a proof of concept, demonstrating that this approach, when optimized, should enable the fabrication of large area CVD-grown heterostructures with excellent optical quality.

Previous attempts at improving the optical properties of CVD-grown $MoSe_2$ using HBr treatment[29] or the isoelectronic impurity substitution[30] have met with only partial success; impurity-bound excitons still remained the most prominent component of the emission spectrum. Low-temperature PL spectra consisted in broad features, wherein free exciton emission could be identified only after fitting. The optical properties of exfoliated MoS_2 have been improved by superacid treatment.[51] In our case, the simple act of bringing $MoSe_2$ in intimate physical contact with MoS_2, a procedure that can be performed after growth and does not require any chemical functionalization, results in a virtually complete suppression of emission from the impurity-bound states and a spectrum in which the trion and exciton resonances can be clearly resolved.

Our defect healing hypothesis is further supported by the results obtained from DFT simulations. We have calculated the gain of energy in a heterobilayer $MoSe_2/MoS_2$ using two models: A single Se vacancy in the $MoSe_2$ layer (Model 1) and a single S vacancy in the MoS_2 layer together with a single S substitution in the $MoSe_2$ layer (Model 2). This corresponds to the transfer energy of a S atom from pristine MoS_2 to heal a defect in $MoSe_2$. We observe a significant energy gain of 18 kJ mol^{-1} (180 meV) per S transfer from MoS_2 to the $MoSe_2$ defect, which shows that defect healing in $MoSe_2$ by MoS_2 is thermodynamically favored. The formation energy of a S vacancy in a MoS_2 monolayer has been theoretically estimated in the 1.3–1.5 eV range.[52,53] We consider these as upper bounds for the energy barrier of the transfer of a S atom to fill a Se vacancy in $MoSe_2$, because this is not a static process but a transfer between two neighboring layers.

We have also calculated the band structures of a perfect $MoSe_2$ monolayer, $MoSe_2$ monolayer with one Se vacancy, and $MoSe_2$ monolayer with one Se→S substitution. We observe that Se vacancies introduce strongly localized states in the bandgap of $MoSe_2$, 0.92 eV above the top of the valence band (see Figure 2). These are dispersionless and act as trap centers. Healing the Se vacancy with S substitution restores the band structure of a nearly perfect $MoSe_2$ monolayer. In the studied 5 × 5 supercell model (2% Se→S substitutions), the bandgap increases by only 1 meV.

Charge Transfer-Mediated Valley Polarization. First signatures of charge transfer between the layers are seen in the comparison between PL intensities of as grown layers and trilayers, shown in Figure S2 of SI. Additional insights is provided by the spatial correlation of the PL intensity of the

DOI: 10.1021/acs.nanolett.7b00904
Nano Lett. XXXX, XXX, XXX–XXX

MoS_2 and $MoSe_2$. The integrated spatial map of the $MoSe_2$ A exciton is shown in Figure 3a. The signal is particularly intense

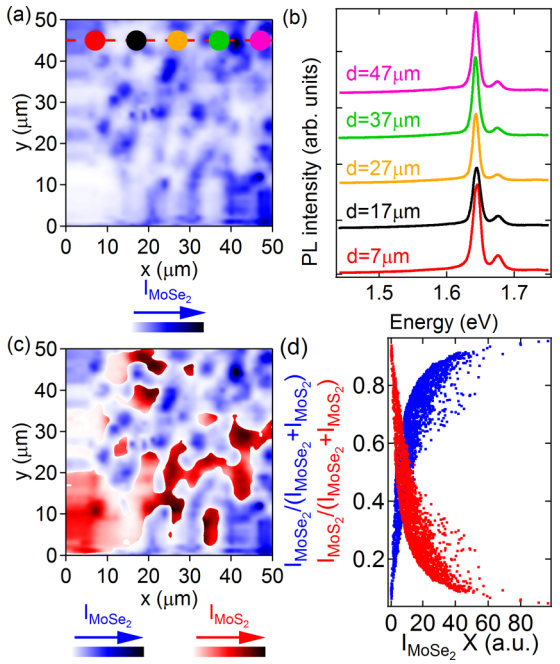

Figure 3. (a) Spatial map of the integrated intensity of A exciton of encapsulated $MoSe_2$. The dashed line schematically illustrates the direction along which the spectra of panel b have been extracted. The colored circles mark the position within the map of the spectra having the corresponding color in panel b. (b) μPL spectra extracted at positions marked by circles of the corresponding color in panel a. The spectra are vertically offset for clarity. (c) Mapping of the integrated intensity of MoS_2 X_A overlaid on the same spatial map of $MoSe_2$ X_A. (d) Integrated intensity of $MoSe_2$ X_A and MoS_2 X_A as a function of the intensity of $MoSe_2$ X_A.

at positions where the overlap between the three layers is good and the material does not have a large number of defects. This implies that the bright spots do not necessarily have a triangular shape. This map provides an additional opportunity to demonstrate the high degree of uniformity of the emission of $MoSe_2$ incorporated in a heterostructure, by extracting μPL spectra. We show in Figure 3b five μPL spectra measured at 10 μm distance from one another. The spectra have been normalized by the integration time. We note that emission from defect states is consistently absent in the five spectra and the similar line shape points to a good uniformity of the emission over the full mapped area. In Figure 3c, we overlay the intensity map of MoS_2 with that of $MoSe_2$, forcing the areas having the lowest signal from the latter to be transparent. These areas correspond to zones where the signal from MoS_2 is highest. We quantify the observed intensity (anti)correlation by plotting in Figure 3d the ratio between the intensity of A exciton in one material normalized by the total emission of both materials $[I_{MoX_2}/(I_{MoS_2} + I_{MoSe_2})$, where X = S or Se$]$. It can be noted that when the emission of $MoSe_2$ becomes more pronounced, the emission of MoS_2 decreases correspondingly. This is fully consistent with charge transfer. In positions where the three layers overlap efficiently, charge transfer induces a quenching of the MoS_2 PL. At the same time, the PL from $MoSe_2$ is particularly intense at these positions owing to efficient defect healing, but still weaker than in as-grown $MoSe_2$ samples (see Figure S2 in SI).

Photoluminescence excitation (PLE) spectroscopy is a useful tool to investigate more thoroughly the charge transfer processes. We focus our measurements on $MoSe_2$ incorporated in a trilayer stack. In Figure 4a, we show the PLE measured without making use of polarization optics. Both PLEs of the A exciton and trion have been normalized by the weakest intensity measured at an excitation energy of 1.999 eV in order to be able to compare the enhancement effects for the exciton and trion. The integrated intensities of both peaks show a pronounced maximum when the excitation energy is close to the resonance with the B exciton of $MoSe_2$.[54] The integrated intensity is consistently lower than this maximum at other excitation energies, including those corresponding to resonances in MoS_2 (see, for example, the weak peak corresponding to MoS_2 X_A, appearing as a shoulder of the main PLE peak in Figure 4a). This is the exact opposite of what is observed in a heterostructure system where energy transfer has been

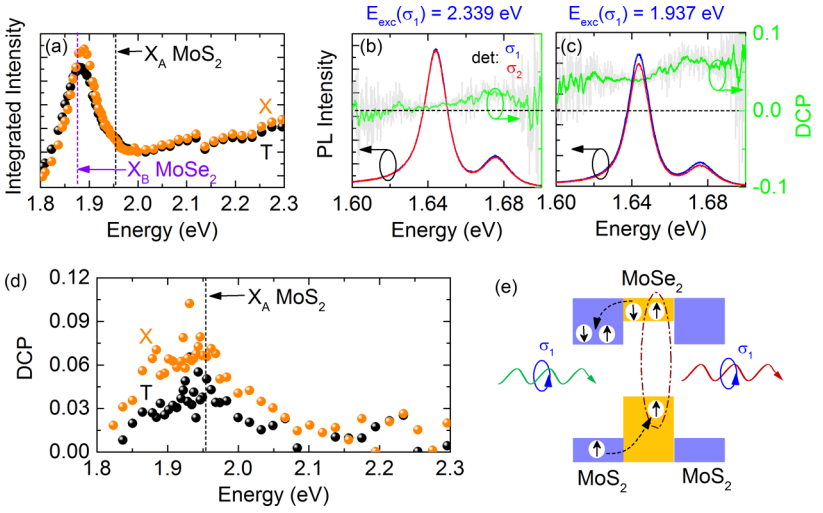

Figure 4. (a) Normalized integrated intensity of $MoSe_2$ X_A and T as a function of the excitation energy. Polarization-resolved μPL spectra and DCP of $MoSe_2$ excited (b) far off MoS_2 X_A resonance and (c) on resonance with MoS_2 X_A. (d) Integrated DCP as a function of the excitation energy. (e) Schematic illustration of spin transfer under excitation resonant with MoS_2 X_A.

DOI: 10.1021/acs.nanolett.7b00904
Nano Lett. XXXX, XXX, XXX−XXX

demonstrated. In such system, the emission intensity of one material is significantly enhanced when the excitation energy is resonant with excitonic transitions of the other material.[55] This consideration allows us to safely rule out energy transfer between the different layers.

To investigate whether the trilayer stack shows charge transfer, we initially consider the normalized intensity of exciton and trion when the excitation energy is resonant with excitonic transitions of MoS_2. For resonances with both A and B exciton of MoS_2, the emission intensity is enhanced more for $MoSe_2$ A exciton than for the trion. This is consistent with the presence of a large n-type background doping (free electrons) in CVD-grown $MoSe_2$, which gives rise to strong charged exciton emission even in the absence of gating (see Figure 1a). For a $MoS_2/MoSe_2$ heterojunction, the band alignment promotes the transfer of holes from MoS_2 to $MoSe_2$.[35] When we optically excite the trilayer stack, we induce a net transfer of holes from MoS_2 to $MoSe_2$, resulting in a relatively stronger emission of the neutral exciton as compared to the trion.[55]

We also performed circular polarization resolved PLE focusing on $MoSe_2$ incorporated in a trilayer stack. When the excitation energy is far from resonance (A or B excitons of both materials), $MoSe_2$ shows an extremely small valley polarization. This is illustrated by the polarization-resolved μPL spectra of Figure 4b, where a negligibly small DCP, defined as DCP = $[I_{\sigma 1} - I_{\sigma 2}]/[I_{\sigma 1} + I_{\sigma 2}]$, is observed across the entire energy range of interest.[38] When the excitation energy of the laser is tuned to the proximity of the resonance with the A exciton of MoS_2, a significant valley polarization accumulates. An example of polarization-resolved spectra at an excitation energy resonant with A exciton of MoS_2 is shown in Figure 4c. The valley polarization is quantified by a slightly positive DCP at energies around A exciton and trion of $MoSe_2$ (see Figure 4c). In Figure 4d, we illustrate the excitation energy dependence of the integrated DCP (estimated by extracting the relevant integrated intensity of exciton and trion with Gaussian fits). We notice a significant increase of the integrated DCP at energies corresponding to the A exciton resonance of MoS_2 (see dashed line in Figure 4d) with a low energy shoulder possibly related to an enhanced DCP at excitation energies corresponding to $MoSe_2$ B exciton.[38] Polarization-resolved electroluminescence of single and multilayer $MoSe_2$[56] as well as polarization-resolved PL of indirect excitons emitted by a $WSe_2/MoSe_2$ heterostructure[57] have demonstrated higher degree of circular polarization. However, the mechanisms leading to polarized emission in these systems are fundamentally different from those yielding polarized PL of $MoSe_2$,[56] which is virtually impossible to achieve unless the PL is excited using quasi-resonant excitation in X_A of $MoSe_2$.[38−40]

We ascribe the observed $MoSe_2$ valley polarization to the hole transfer from MoS_2 with a mechanism schematically illustrated in Figure 4e. We excite the trilayer stack with circularly polarized light with a given helicity and in resonance with the A exciton of MoS_2. The valley polarization directly created in $MoSe_2$ is quickly lost, which results in a negligible DCP, similarly to nonresonant excitation (see Figure 4d). Resonant excitation in MoS_2 creates valley polarization for a duration estimated in the hundreds of femtoseconds range.[58] Charge transfer in van der Waals heterostructures is an ultrafast process with upper bounds in the tens of femtoseconds range (hole transfer from MoS_2 has been reported to be faster than 50 fs[36]). During this very rapid transfer, we assume that the hole spin (and thus valley due to the large spin orbit splitting in the valence band) is conserved, and because of the excess electron population in the $MoSe_2$ layer, the injected hole forms an exciton populating the valley corresponding to the helicity of the incoming light. These excitons have presumably a low kinetic energy (no excess energy of the photocreated hole), which slows down significantly the intervalley scattering rate due to electron−hole exchange interaction.[59] As a result, this hole transfer is responsible for the observed valley polarization.

Conclusions. A detailed investigation of the optical properties of $MoS_2/MoSe_2/MoS_2$ trilayers reveals that stacking dramatically improves the optical quality of CVD-grown $MoSe_2$, essentially eliminating all defect bound exciton and MoS_2-related emission. These results open the way to using CVD-grown TMDCs for applications and studies that require materials with excellent optical quality. Photoluminescence spectra from $MoSe_2$ in a trilayer stack are dominated by narrow neutral and charged A exciton emission, resembling the spectrum of a high quality mechanically exfoliated flake. Density functional calculations confirm a defect healing scenario in which S atoms replace Se vacancies. Circular polarization resolved PL measurements demonstrate that $MoSe_2$ exhibits a significant valley polarization even when the excitation energy is far from the A exciton resonance. This behavior is the signature of an efficient spin-conserving hole transfer from MoS_2 to $MoSe_2$. Our approach provides a robust and straightforward method of healing defects in CVD-grown samples, which might also be beneficial for the transport properties of these materials.

Methods. *Sample Preparation.* The sample with $MoS_2/MoSe_2/MoS_2$ trilayer stacks, schematically shown in Figure 1a, was obtained by two separate transfer steps using a wet transfer KOH method.[32] First of all, the upper-MoS_2 was transferred onto the as-grown $MoSe_2$ monlayer on sapphire.[24,34] Subsequently, the $MoS_2/MoSe_2$ stack was transferred onto an as-grown bottom MoS_2 monolayer on sapphire. For both transfers, sapphire chips with material (upper-MoS_2 or $MoS_2/MoSe_2$ stack) were first spin coated with PMMA 950 at 1500 rpm for 60 s and baked at 180 °C for 5 min. The films were detached in KOH (30%) at moderate temperatures (70 °C), washed three times in deionized water, transferred onto sapphire with the stacking layer ($MoSe_2$ or bottom-MoS_2), and dried at 50 °C for 30 min. The PMMA was removed by dipping the sample in acetone for 12 h, followed by rinsing with isopropanol and drying in a N_2 flow. Such method provides a polymer clean interface of stacks and minimal damage of material caused by the transfer process. Using this method, a large area film with monolayer (MoS_2), bilayer ($MoSe_2/MoS_2$, MoS_2/MoS_2, and $MoS_2/MoSe_2$ stacks) and trilayer ($MoS_2/MoSe_2/MoS_2$ stack) was obtained. A micrograph of a representative transfer area is shown in Figure 1b. To determine the position of areas with different number of stacked layers, Ni markers were deposited.

Optical Measurements. For the optical characterization, the sapphire substrate was mounted on the cold finger of a He-flow croystat. The excitation was provided either by a CW frequency-doubled solid-state laser emitting at 532 nm or by the frequency-doubled output of an optical parametric oscillator (OPO), synchronously pumped by a mode-locked Ti:sapphire laser. The typical temporal pulse width was 300 fs, with a repetition rate of 80 MHz. The excitation beam was focused on the sample by a 50× microscope objective, giving a spot size of approximately 1 μm and having a numerical aperture of 0.55. The emitted PL was collected through the

DOI: 10.1021/acs.nanolett.7b00904
Nano Lett. XXXX, XXX, XXX−XXX

same objective and redirected to a spectrometer equipped with a liquid nitrogen cooled CCD camera or (for time-resolved measurements) to an imagining spectrometer and detected using a synchroscan streak camera with the temporal resolution set to 5 ps. All the spectra have been measured at 5K, unless otherwise specified.

For spatial mapping the emission has been monitored while the optical cryostat was displaced with respect to the microscope objective using high precision motorized $x-y$ translation stages (1 μm step). The integrated intensity of given features (e.g., A exciton emission) has been obtained by performing Gaussian fitting of the measured μPL spectra.

Density Functional Theory of Band Structure in $MoSe_2$/MoS_2 Heterobilayers. We have calculated heterobilayers made of $MoSe_2$ and MoS_2 monolayers, using DFT as implemented in the Crystal09 software.[60] We employed all-electron Gaussian-type bases of triple-quality,[61,62] while Mo atoms were treated with the HAYWSC-311(d31)G basis with effective core potential set,[63] together with the PBE gradient corrected density functional.[64] London-dispersion interactions were accounted for using the approach proposed by Grimme (DFT-D3).[65] Full optimization of atomic positions and lattice vectors was performed on both models: Model 1 with perfect MoS_2 monolayer and one Se vacancy in the $MoSe_2$ monolayer, and Model 2 with one S vacancy in the MoS_2 monolayer and one S substitution in the $MoSe_2$ monolayer. The models are built of 5 × 5 supercells (see Figure 2).

Geometry optimization only slightly alters the lattice geometry (see Table 1).

Table 1. Structural Parameters of MoS_2/$MoSe_2$ Defective Heterostructures Giving the Lattice Constant (a) and Interlayer Metal-to-Metal Distances (d)

System	a (Å)	d (Å)
MoS_2 1L	3.171	
$MoSe_2$ 1L	3.251	
MoS_2/$MoSe_2$	3.214	6.21
Model 1	3.206	6.30
Model 2	3.203	6.26

For the large supercells, which still overestimate the defect density in experiment, the defects studied here do not introduce any drastic changes into the structural properties of the systems. However, we note that we are constrained with the commensurate models of a heterobilayer, in which the corresponding monolayers are slightly distorted compared with the relaxed monolayers 3.251 and 3.171 Å for $MoSe_2$ and MoS_2, respectively. For a perfect heterobilayer (3.214 Å), this gives 1.15% compression of $MoSe_2$ and 1.4% elongation of MoS_2.

■ ASSOCIATED CONTENT

Supporting Information

The Supporting Information is available free of charge on the ACS Publications website at DOI: 10.1021/acs.nanolett.7b00904.

Low-temperature μPL spectra, comparison of μPL spectra of as-grown versus trilayer samples, temperature-dependent μPL spectra, and time-resolved PL (PDF)

■ AUTHOR INFORMATION

Corresponding Author

*E-mail: paulina.plochocka@lncmi.cnrs.fr.

ORCID

Thomas Heine: 0000-0003-2379-6251

Andras Kis: 0000-0002-3426-7702

Paulina Plochocka: 0000-0002-4019-6138

Notes

The authors declare no competing financial interest.

■ ACKNOWLEDGMENTS

This work was partially supported by ANR JCJC project milliPICS, the Région Midi-Pyrénées under contract MESR 13053031, BLAPHENE project under IDEX program Emergence, "Programme des Investissements d'Avenir" under the program ANR-11-IDEX-0002-02, reference ANR-10-LABX-0037-NEXT, Swiss SNF Sinergia Grant 147607, the European Commission (ITN MoWSeS, GA 317451), and Deutsche Forschungsgemeinschaft (HE 3543/27-1 and GRK 2247/1 (QM3)). Y.J., A.K., and T.H. thank ZIH Dresden for supercomputer time. This project has received funding from the European Union's Horizon 2020 research and innovation programme under Grant 696656 (Graphene Flagship).

■ REFERENCES

(1) Splendiani, A.; Sun, L.; Zhang, Y.; Li, T.; Kim, J.; Chim, C.-Y.; Galli, G.; Wang, F. *Nano Lett.* **2010**, *10*, 1271−1275.

(2) Mak, K. F.; Lee, C.; Hone, J.; Shan, J.; Heinz, T. F. *Phys. Rev. Lett.* **2010**, *105*, 136805.

(3) Radisavljevic, B.; Radenovic, A.; Brivio, J.; Giacometti, V.; Kis, A. *Nat. Nanotechnol.* **2011**, *6*, 147−150.

(4) Kuc, A.; Zibouche, N.; Heine, T. *Phys. Rev. B: Condens. Matter Mater. Phys.* **2011**, *83*, 245213.

(5) Lopez-Sanchez, O.; Lembke, D.; Kayci, M.; Radenovic, A.; Kis, A. *Nat. Nanotechnol.* **2013**, *8*, 497−501.

(6) Baugher, B. W.; Churchill, H. O.; Yang, Y.; Jarillo-Herrero, P. *Nat. Nanotechnol.* **2014**, *9*, 262−267.

(7) Ross, J. S.; Klement, P.; Jones, A. M.; Ghimire, N. J.; Yan, J.; MandrusD, G.; Taniguchi, T.; Watanabe, K.; Kitamura, K.; Yao, W.; Cobden, D. H.; Xu, X. *Nat. Nanotechnol.* **2014**, *9*, 268−272.

(8) Pospischil, A.; Furchi, M. M.; Mueller, T. *Nat. Nanotechnol.* **2014**, *9*, 257−261.

(9) Koppens, F. H. L.; Mueller, T.; Avouris, P.; Ferrari, A. C.; Vitiello, M. S.; Polini, M. *Nat. Nanotechnol.* **2014**, *9*, 780−793.

(10) Mak, K. F.; Shan, J. *Nat. Photonics* **2016**, *10*, 216−226.

(11) Cao, T.; Wang, G.; Han, W.; Ye, H.; Zhu, C.; Shi, J.; Niu, Q.; Tan, P.; Wang, E.; Liu, B.; Ji, F. *Nat. Commun.* **2012**, *3*, 887.

(12) Zeng, H.; Dai, J.; Yao, W.; Xiao, D.; Cui, X. *Nat. Nanotechnol.* **2012**, *7*, 490−493.

(13) Mak, K. F.; He, K.; Shan, J.; Heinz, T. F. *Nat. Nanotechnol.* **2012**, *7*, 494−498.

(14) Li, Y.; Chernikov, A.; Zhang, X.; Rigosi, A.; Hill, H. M.; van der Zande, A. M.; Chenet, D. A.; Shih, E.-M.; Hone, J.; Heinz, T. F. *Phys. Rev. B: Condens. Matter Mater. Phys.* **2014**, *90*, 205422.

(15) He, K.; Kumar, N.; Zhao, L.; Wang, Z.; Mak, K. F.; Zhao, H.; Shan, J. *Phys. Rev. Lett.* **2014**, *113*, 026803.

(16) Mak, K. F.; He, K.; Lee, C.; Lee, G. H.; Hone, J.; Heinz, T. F.; Shan, J. *Nat. Mater.* **2012**, *12*, 207−211.

(17) Xiao, D.; Liu, G.-B.; Feng, W.; Xu, X.; Yao, W. *Phys. Rev. Lett.* **2012**, *108*, 196802.

(18) Jones, A. M.; Yu, H.; Ghimire, N. J.; Wu, S.; Aivazian, G.; Ross, J. S.; Zhao, B.; Yan, J.; Mandrus, D. G.; Xiao, D.; Yao, W.; Xu, X. *Nat. Nanotechnol.* **2013**, *8*, 634−638.

(19) Plechinger, G.; Nagler, P.; Kraus, J.; Paradiso, N.; Strunk, C.; Schüller, C.; Korn, T. *Phys. Status Solidi RRL* **2015**, *9*, 457−461.

DOI: 10.1021/acs.nanolett.7b00904
Nano Lett. XXXX, XXX, XXX−XXX

(20) Wang, G.; Marie, X.; Gerber, I.; Amand, T.; Lagarde, D.; Bouet, L.; Vidal, M.; Balocchi, A.; Urbaszek, B. *Phys. Rev. Lett.* **2015**, *114*, 097403.
(21) Srivastava, A.; Sidler, M.; Allain, A. V.; Lembke, D. S.; Kis, A.; Imamoğlu, A. *Nat. Phys.* **2015**, *11*, 141−147.
(22) Zhu, Z. Y.; Cheng, Y. C.; Schwingenschlögl, U. *Phys. Rev. B: Condens. Matter Mater. Phys.* **2011**, *84*, 153402.
(23) Zhan, Y.; Liu, Z.; Najmaei, S.; Ajayan, P. M.; Lou, J. *Small* **2012**, *8*, 966−971.
(24) Dumcenco, D.; Ovchinnikov, D.; Marinov, K.; Lazic, P.; Gibertini, M.; Marzari, N.; Sanchez, O. L.; Kung, Y.-C.; Krasnozhon, D.; Chen, M.-W.; Bertolazzi, S.; Gillet, P.; Fontcuberta i Morral, A.; Radenovic, A.; Kis, A. *ACS Nano* **2015**, *9*, 4611−4620.
(25) Wang, X.; Gong, Y.; Shi, G.; Chow, W. L.; Keyshar, K.; Ye, G.; Vajtai, R.; Lou, J.; Liu, Z.; Ringe, E.; Tay, B. K.; Ajayan, P. M. *ACS Nano* **2014**, *8*, 5125−5131.
(26) Zhang, Y.; Zhang, Y.; Ji, Q.; Ju, J.; Yuan, H.; Shi, J.; Gao, T.; Ma, D.; Liu, M.; Chen, Y.; Song, X.; Hwang, H. Y.; Liu, Z. *ACS Nano* **2013**, *7*, 8963−8971.
(27) Huang, J.-K.; Pu, J.; Hsu, C.-L.; Chiu, M.-H.; Juang, Z.-Y.; Chang, Y.-H.; Chang, W.-H.; Iwasa, Y.; Takenobu, T.; Li, L.-J. *ACS Nano* **2014**, *8*, 923−930.
(28) Chang, Y.-H.; et al. *ACS Nano* **2014**, *8*, 8582−8590.
(29) Han, H.-V.; Lu, A.-Y.; Lu, L.-S.; Huang, J.-K.; Li, H.; Hsu, C.-L.; Lin, Y.-C.; Chiu, M.-H.; Suenaga, K.; Chu, C.-W.; Kuo, H.-C.; Chang, W.-H.; Li, L.-J.; Shi, Y. *ACS Nano* **2016**, *10*, 1454−1461.
(30) Li, X.; Puretzky, A. A.; Sang, X.; KC, S.; Tian, M.; Ceballos, F.; Mahjouri-Samani, M.; Wang, K.; Unocic, R. R.; Zhao, H.; Duscher, G.; Cooper, V. R.; Rouleau, C. M.; Geohegan, D. B.; Xiao, K. *Adv. Funct. Mater.* **2017**, *27*, 1603850.
(31) Chiu, M.-H.; Li, M.-Y.; Zhang, W.; Hsu, W.-T.; Chang, W.-H.; Terrones, M.; Terrones, H.; Li, L.-J. *ACS Nano* **2014**, *8*, 9649−9656.
(32) Wang, K.; Huang, B.; Tian, M.; Ceballos, F.; Lin, M.-W.; Mahjouri-Samani, M.; Boulesbaa, A.; Puretzky, A. A.; Rouleau, C. M.; Yoon, M.; Zhao, H.; Xiao, K.; Duscher, G.; Geohegan, D. B. *ACS Nano* **2016**, *10*, 6612−6622.
(33) Tongay, S.; Fan, W.; Kang, J.; Park, J.; Koldemir, U.; Suh, J.; Narang, D. S.; Liu, K.; Ji, J.; Li, J.; Sinclair, R.; Wu, J. *Nano Lett.* **2014**, *14*, 3185−3190.
(34) Mitioglu, A.; Galkowski, K.; Surrente, A.; Klopotowski, L.; Dumcenco, D.; Kis, A.; Maude, D.; Plochocka, P. *Phys. Rev. B: Condens. Matter Mater. Phys.* **2016**, *93*, 165412.
(35) Kang, J.; Tongay, S.; Zhou, J.; Li, J.; Wu, J. *Appl. Phys. Lett.* **2013**, *102*, 012111.
(36) Hong, X.; Kim, J.; Shi, S.-F.; Zhang, Y.; Jin, C.; Sun, Y.; Tongay, S.; Wu, J.; Zhang, Y.; Wang, F. *Nat. Nanotechnol.* **2014**, *9*, 682−686.
(37) Ceballos, F.; Bellus, M. Z.; Chiu, H.-Y.; Zhao, H. *ACS Nano* **2014**, *8*, 12717−12724.
(38) Wang, G.; Palleau, E.; Amand, T.; Tongay, S.; Marie, X.; Urbaszek, B. *Appl. Phys. Lett.* **2015**, *106*, 112101.
(39) Kioseoglou, G.; Hanbicki, A. T.; Currie, M.; Friedman, A. L.; Jonker, B. T. *Sci. Rep.* **2016**, *6*, 25041.
(40) Baranowski, M.; Surrente, A.; Maude, D.; Ballottin, M.; Mitioglu, A.; Christianen, P.; Dumcenco, D.; Kung, Y.-C.; Kis, A.; Plochocka, P. *2D Mater.* **2017**, *4*, 025016.
(41) Tongay, S.; Suh, J.; Ataca, C.; Fan, W.; Luce, A.; Kang, J. S.; Liu, J.; Ko, C.; Raghunathanan, R.; Zhou, J.; Ogletree, F.; Li, J.; Grossman, J. C.; Wu, J. *Sci. Rep.* **2013**, *3*, 2657.
(42) Rigosi, A. F.; Hill, H. M.; Li, Y.; Chernikov, A.; Heinz, T. F. *Nano Lett.* **2015**, *15*, 5033−5038.
(43) Ramasubramaniam, A. *Phys. Rev. B: Condens. Matter Mater. Phys.* **2012**, *86*, 115409.
(44) Withers, F.; et al. *Nano Lett.* **2015**, *15*, 8223−8228.
(45) Dumcenco, D.; Ovchinnikov, D.; Marinov, K.; Kis, A. High-quality synthetic 2D transition metal dichalcogenide semiconductors. *46th European Solid-State Device Research Conference (ESSDERC), Lausanne*; 2016; pp 284−286 DOI: 10.1109/ESSDERC.2016.7599641.
(46) Ross, J. S.; Wu, S.; Yu, H.; Ghimire, N. J.; Jones, A. M.; Aivazian, G.; Yan, J.; Mandrus, D. G.; Xiao, D.; Yao, W.; Xu, X. *Nat. Commun.* **2013**, *4*, 1474.
(47) Arora, A.; Nogajewski, K.; Molas, M.; Koperski, M.; Potemski, M. *Nanoscale* **2015**, *7*, 20769−20775.
(48) Yu, Y.; Hu, S.; Su, L.; Huang, L.; Liu, Y.; Jin, Z.; Purezky, A. A.; Geohegan, D. B.; Kim, K. W.; Zhang, Y.; Cao, L. *Nano Lett.* **2015**, *15*, 486−491.
(49) Tongay, S.; Zhou, J.; Ataca, C.; Lo, K.; Matthews, T. S.; Li, J.; Grossman, J. C.; Wu, J. *Nano Lett.* **2012**, *12*, 5576−5580.
(50) Tonndorf, P.; Schmidt, R.; Böttger, P.; Zhang, X.; Börner, J.; Liebig, A.; Albrecht, M.; Kloc, C.; Gordan, O.; Zahn, D. R.; Michaelis de Vasconcellos, S.; Bratschitsch, R. *Opt. Express* **2013**, *21*, 4908−4916.
(51) Cadiz, F.; Tricard, S.; Gay, M.; Lagarde, D.; Wang, G.; Robert, C.; Renucci, P.; Urbaszek, B.; Marie, X. *Appl. Phys. Lett.* **2016**, *108*, 251106.
(52) Noh, J.-Y.; Kim, H.; Kim, Y.-S. *Phys. Rev. B: Condens. Matter Mater. Phys.* **2014**, *89*, 205417.
(53) Komsa, H.-P.; Krasheninnikov, A. V. *Phys. Rev. B: Condens. Matter Mater. Phys.* **2015**, *91*, 125304.
(54) Kozawa, D.; Kumar, R.; Carvalho, A.; Amara, K. K.; Zhao, W.; Wang, S.; Toh, M.; Ribeiro, R. M.; Neto, A. C.; Matsuda, K.; Eda, G. *Nat. Commun.* **2014**, *5*, 4543.
(55) Kozawa, D.; Carvalho, A.; Verzhbitskiy, I.; Giustiniano, F.; Miyauchi, Y.; Mouri, S.; Castro Neto, A.; Matsuda, K.; Eda, G. *Nano Lett.* **2016**, *16*, 4087−4093.
(56) Onga, M.; Zhang, Y.; Suzuki, R.; Iwasa, Y. *Appl. Phys. Lett.* **2016**, *108*, 073107.
(57) Rivera, P.; Seyler, K. L.; Yu, H.; Schaibley, J. R.; Yan, J.; Mandrus, D. G.; Yao, W.; Xu, X. *Science* **2016**, *351*, 688−691.
(58) Mai, C.; Barrette, A.; Yu, Y.; Semenov, Y. G.; Kim, K. W.; Cao, L.; Gundogdu, K. *Nano Lett.* **2014**, *14*, 202−206.
(59) Yu, T.; Wu, M. *Phys. Rev. B: Condens. Matter Mater. Phys.* **2014**, *89*, 205303.
(60) Dovesi, R.; Saunders, V. R.; Roetti, R.; Orlando, R.; Zicovich-Wilson, C. M.; Pascale, F.; Civalleri, B.; Doll, K.; Harrison, N. M.; Bush, I. J.; D'Arco, P.; Llunell, M. *CRYSTAL09 User's Manual*; University of Torino: Torino, Italy, 2009.
(61) Peintinger, M. F.; Oliveira, D. V.; Bredow, T. *J. Comput. Chem.* **2013**, *34*, 451−459.
(62) Lichanot, A.; Apra, E.; Dovesi, R. *Phys. Status Solidi B* **1993**, *177*, 157−163.
(63) Cora, F.; Patel, A.; Harrison, N. M.; Roetti, C.; Richard, A.; Catlow, C. *J. Mater. Chem.* **1997**, *7*, 959−967.
(64) Perdew, J. P.; Burke, K.; Ernzerhof, M. *Phys. Rev. Lett.* **1996**, *77*, 3865−3868.
(65) Grimme, S. *J. Comput. Chem.* **2006**, *27*, 1787−1799.

DOI: 10.1021/acs.nanolett.7b00904
Nano Lett. XXXX, XXX, XXX−XXX